Extended Data for

Tlr7-biallelism defines a hyperfunctional state of female B lymphocytes

Charles-Henry Miquel, Mélissa Nieucel, Léa Ferrayé et al.

Corresponding author: Jean-Charles Guéry, PhD
E-mail : jean-charles.guery@inserm.fr

The PDF file includes:

Extended Data Fig. 1 to Fig. 10

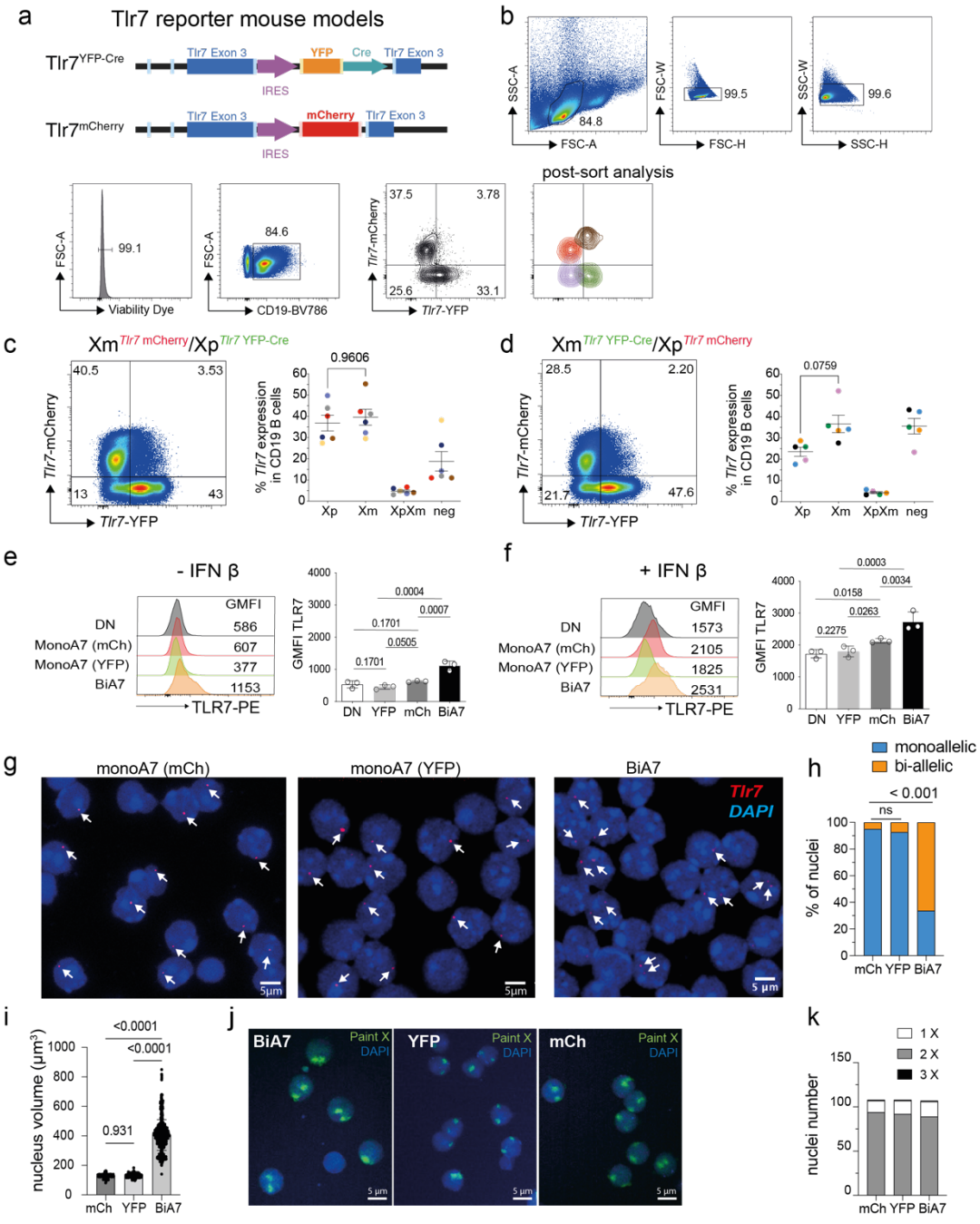

Extended data Figure 1: Characterization of *Tlr7* bi-allelic splenic B cells. (**a**) Design of *Tlr7*-reporter mice. A reporter cassette including an IRES followed by a fluorescent protein (mCherry or YFP-Cre) was inserted at the 3' end of the endogenous *Tlr7* gene. (**b**) Gating strategy for cell-sorting of MonoA7 (mCherry or YFP), BiA7 (mCherry^{+}/YFP^{+}) and double negative (DN) CD19^{+} B cells. Representative flow cytometry purity profile from cell sorting experiment is shown. (**c, d**) Representative flow cytometry plot and quantification of *Tlr7*-reporter allelic expression from splenic CD19^{+} B cells from Xm$^{Tlr7\text{-}mCherry}$Xp$^{Tlr7\text{-}YFP\text{-}Cre}$ (**c**) or the reverse crossing Xm$^{Tlr7\text{-}YFP\text{-}Cre}Xp^{Tlr7\text{-}mCherry}$ (**d**) female mice (maternal X, Xm; paternal X, Xp). (**e,f**) GMFI quantification of intracellular TLR7 staining in FACS-sorted DN, MonoA7 and BiA7 CD19^{+} B cells cultured overnight without (**e**) or with 2 ng/ml IFN-β (**f**). TLR7 staining expressed as ΔGMFI with isotype control. Quantifications are shown from three independent experiments. (**g**) Representative RNA FISH images of *Tlr7* primary transcripts.

Nuclei counterstained with DAPI (blue). Scale bars, 5µm. (**h**) Frequency of mono- and bi-allelic RNA FISH signals within the sorted MonoA7 or BiA7 cell populations. (**i**) Nucleus volume (µm^3) measured by Imaris from MonoA7 and BiA7 B cells. (**j**) Representative images of paint DNA FISH for the X chromosomes (green). Nuclei counterstained with DAPI (blue). Scale bars, 5µm. (**k**) Quantification of the number of X chromosome territories per nucleus in sorted MonoA7 and BiA7 B cells. Statistical analysis was performed using One-way ANOVA with Tukey multiple-comparison test. For (h) statistical differences were assessed using Fisher's exact test or One-way ANOVA with Tukey multiple-comparison test (i). Exact p values are shown.

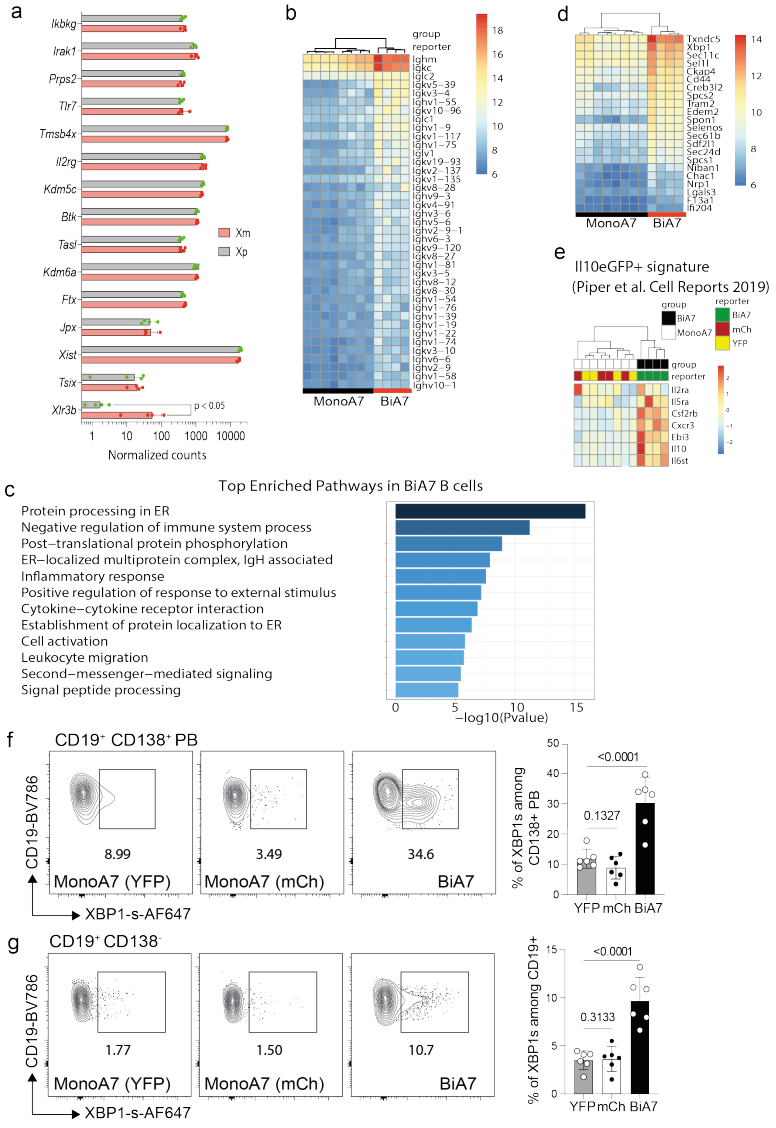

Extended data Figure 2: Characterization of the transcriptional signature of BiA7 B cells. RNA-seq data between BiA7 and MonoA7 B cells (n=4/group). (**a**) Relative expression of the maternally imprinted gene *Xlr3b* compared to 14 representative X-linked genes from individual mice (n=4). Adjusted p value is shown. (**b**) Heatmap representing variance-stabilized normalized counts for Ig-related genes identified as differentially regulated between BiA7 and MonoA7 samples and having an average expression greater than 200 normalized counts in at least 3 of the 4 BiA7 samples. (**c**) Metascape analysis showing the top enriched pathways corresponding to the selected cluster summary terms obtained from 504 non-Ig genes with log2FC >1, pvalue <0.05 with background: 12563 non-Ig expressed genes. (**d**) Heatmap showing the unsupervised clustering of the DEG (log2FC>1, adj. p-value

<0.05) from the pathways underlined in bold panel in (c). (**e**) Heatmap of *Il10*eGFP+ signature genes upregulated in BiA7 B cells with log2FC>1 adj. p-value <0.05. Heatmap rows ordered based on average expression level in BiA7 samples. (**f,g**) Intracellular analysis of XBP1s expression on $CD19^{+}CD138^{+}$ PB (**f**) or $CD19^{+}CD138^{-}$ B cells (**g**) from splenic IgD^{+} MonoA7 or BiA7 B cells sorted and stimulated as in Fig. 1g for 3 days. Statistical analysis was performed using One-way ANOVA with Tukey multiple-comparison test. The symbols represent individual mice; the error bars represent the mean±SD.

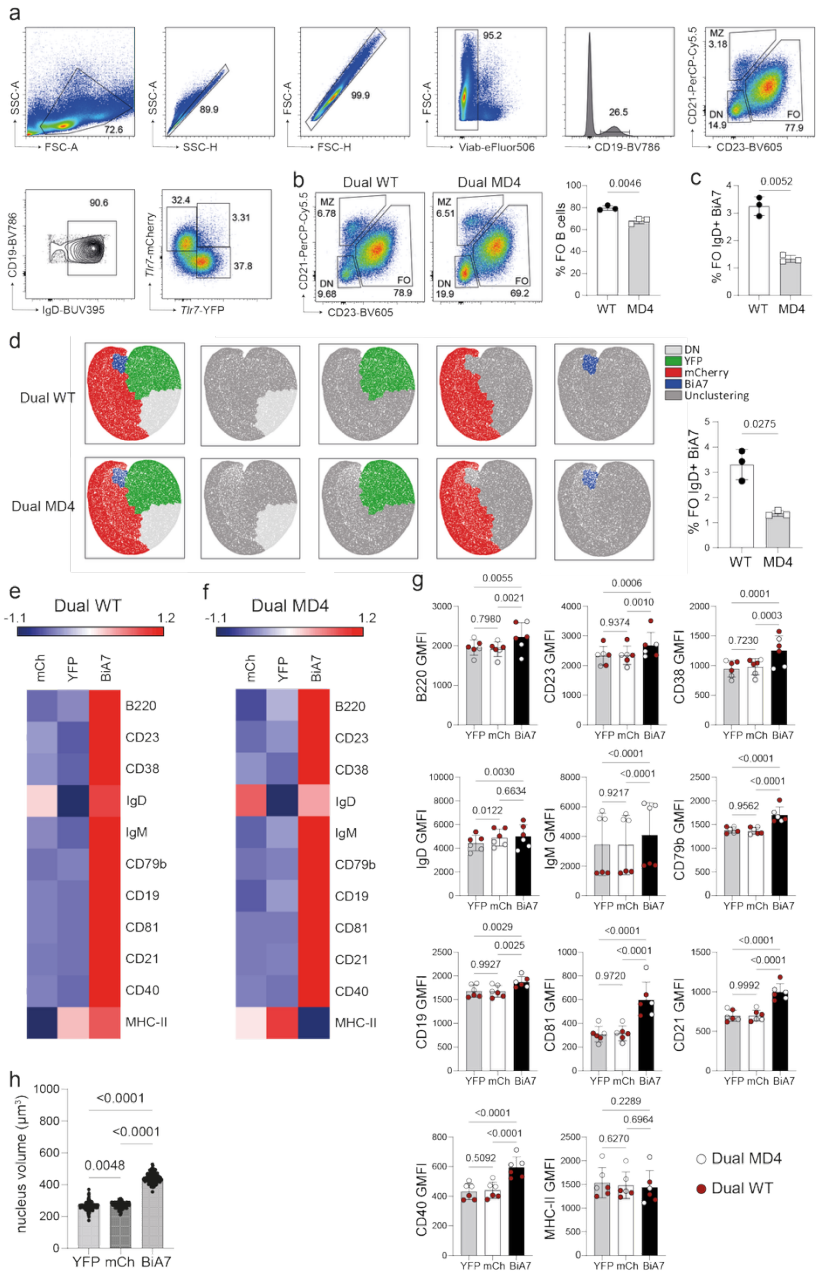

Extended data Figure 3: BCR-specificity does not influence the development of BiA7 B cells.
(**a**) *Ex vivo* gating strategy on splenocytes from Dual WT and Dual MD4 mice. (**b**) Representative cytometry plot of DN, MZ and FO splenic B cells profile and the frequency of FO B cells in Dual WT and Dual MD4 mice. (**c**) Frequency of BiA7 naive FO IgD+ B cells in Dual WT and Dual MD4 mice. (**d**) Reporter-based unsupervised clustering and quantification of BiA7 among FO IgD+ cells in Dual WT and Dual MD4 mice. (**e-g**) Expression of cell surface markers and functional molecules in sorted MonoA7 and BiA7 FO B cells from Dual WT (**e**) or Dual MD4 (**f**) mice. (**g**) Histograms of GMFI of these markers from (**e,f**). (**h**) Nucleus volume (μm^3) measured by Imaris in sorted MonoA7 and BiA7 B cells. Statistical analysis was performed using Welch's t test (**b,c,d**), or One-way ANOVA with Tukey

multiple-comparison test (**g,h**). The symbols represent individual mice; the error bars represent the mean±SD.

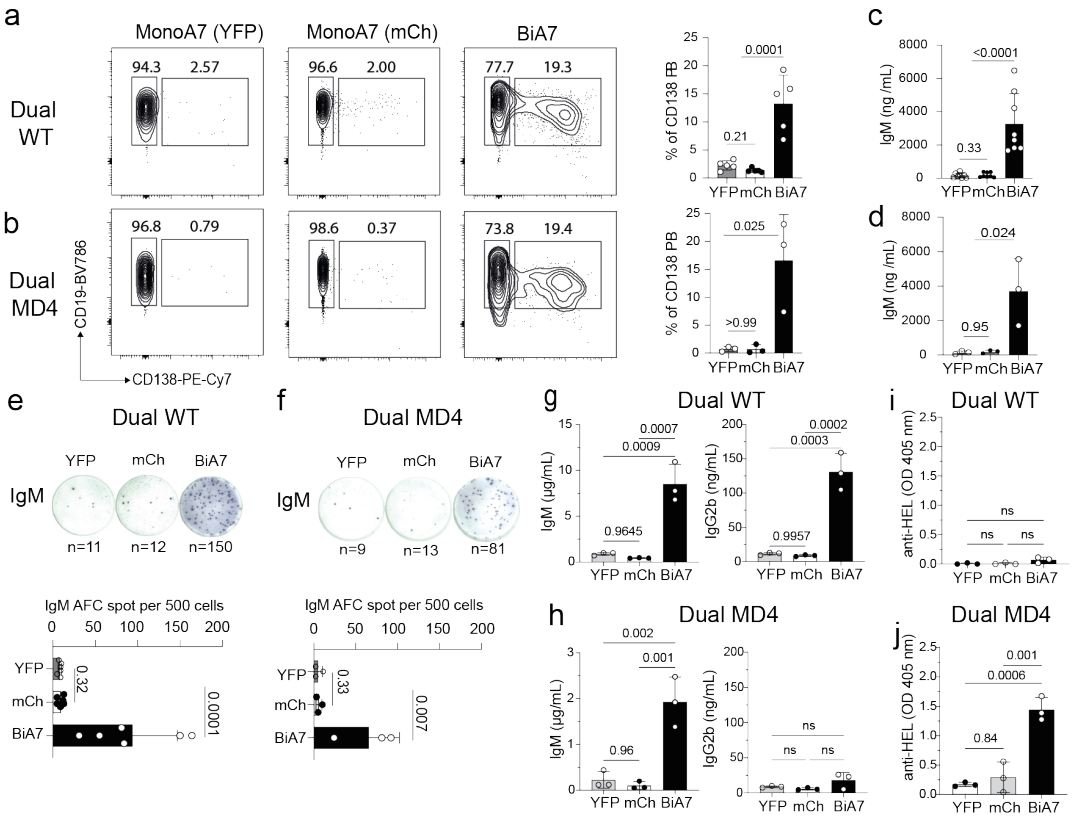

Extended data Figure 4: BiA7 FO B cells with a hyperactive potential developed independently of BCR specificity. (**a, b**) Representative cytometry plot of CD19 CD138 staining and frequency of CD19+CD138+ PB on sorted MonoA7 and BiA7 IgD^{+} FO B cells cultured with F(ab')$_2$ anti-IgM, anti-CD40 and CL097 for 3 days from Dual WT (**a**) and Dual MD4 (**b**) mice. Concentration of IgM collected in supernatants of cultured MonoA7 and BiA7 cells from Dual WT (**c**) and Dual MD4 (**d**) mice assessed by ELISA. Analysis of antibody forming cells (AFC) secreting IgM antibodies from Dual WT (**e**) and Dual MD4 (**f**) assessed by ELISPOT. (**g, i**) Comparative analysis of the production of IgM, class-switched IgG2b (**g, h**) and anti-HEL antibody **(i, j**) between the indicated B cell subsets purified from Dual WT (**g, i**) or Dual MD4 (**h, j**) mice. Statistical analyses were performed using a One Way ANOVA and multiple comparison Dunnett's test. The symbols represent individual mice; the error bars represent the mean±SD.

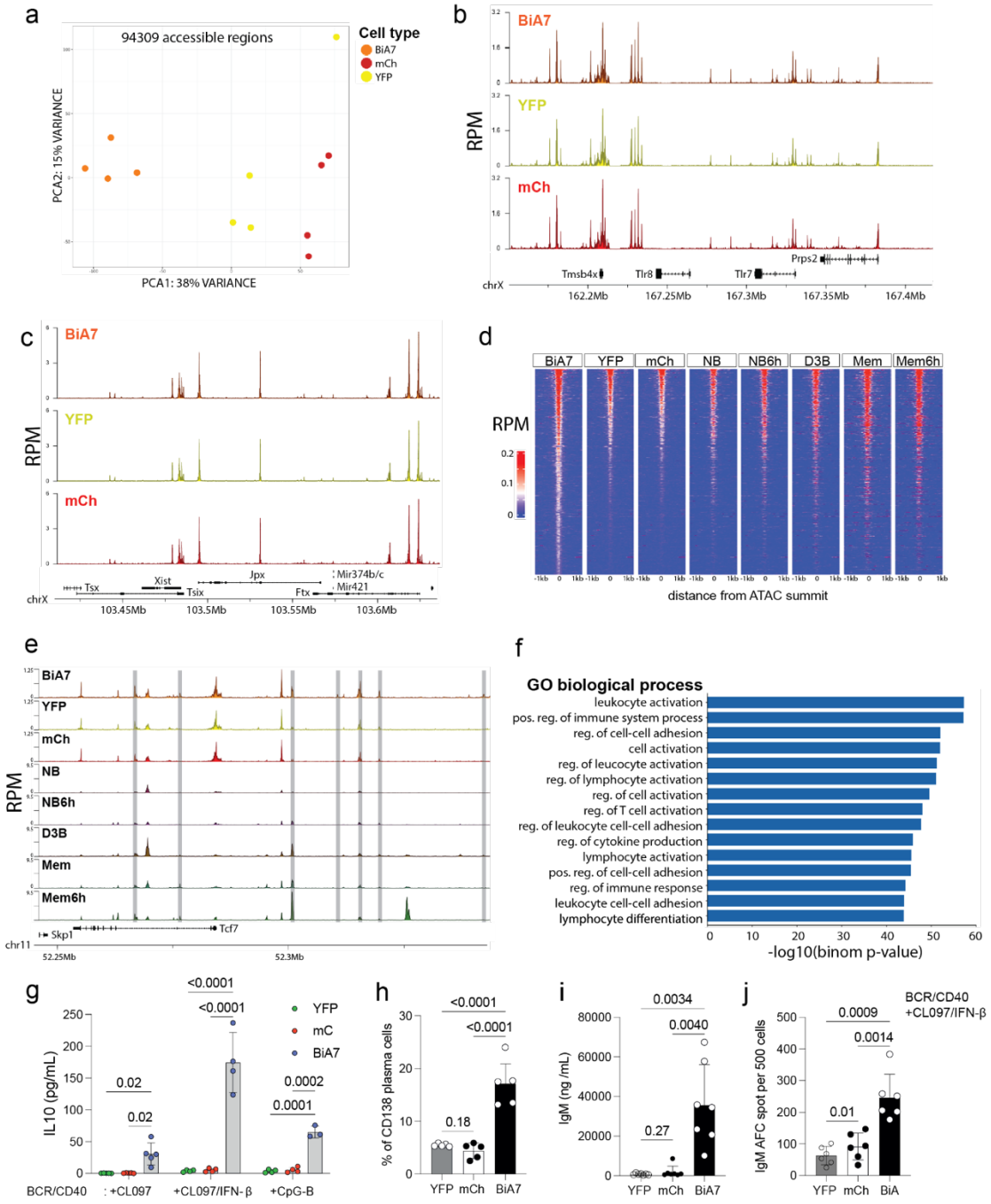

Extended data Figure 5: Accessibility landscape changes in naive BiA7 B cells. (**a**) Principal component analysis of chromatin accessibility across 94309 accessible regions between BiA7 and mCh, YFP MonoA7 B cells. (**b, c**) Chromatin accessibility at the *Tlr7/Tlr8* locus (**b**) and in the *Xist* region (**c**) in BiA7 and MonoA7 B cells. (**d**) Heatmap of chromatin accessibility measured by ATAC-seq across BiA7-specific DARs centered on ATAC-seq summits (+-1kb) in BiA7 cells compared to MonoA7 (YFP or mCh) B cells and as well as in naïve (NB), activated (D3B) and memory (Mem) or activated Mem B cells from Qß-VLP immunized mice. (**e**) Chromatin accessibility at the *Tcf7* locus in the indicated B cell populations. (**f**) Statistical association of GO biological processes with BiA7-specific DARs. (**g**) Quantification of IL-10 production in 3 day-culture supernatants of $CD19^{+}IgD^{+}$ sorted BiA7 and MonoA7 cells stimulated with $F(ab')_2$ goat anti-mouse IgM, anti-CD40, and the indicated TLR ligands, either CL097 for TLR7 (alone or in combination with IFN-ß) or CpG-B for TLR9. (**h-j**) Analysis of $CD19^{+}IgD^{+}$ sorted BiA7 and MonoA7 cells after 3 days of stimulation with $F(ab')_2$ goat anti-mouse

IgM, anti-CD40, CL097 and IFN-ß: Frequency of CD19^{int} CD138^{+} PB (**h**), concentration of IgM (**i**), and frequency of IgM secreting cells assessed by ELISPOT (**j**). One-way ANOVA followed by Sidak's multiple comparisons test was used to compare BiA7 cells with the other groups. The symbols represent individual mice; bars represent the mean; the error bars represent the mean±SD.

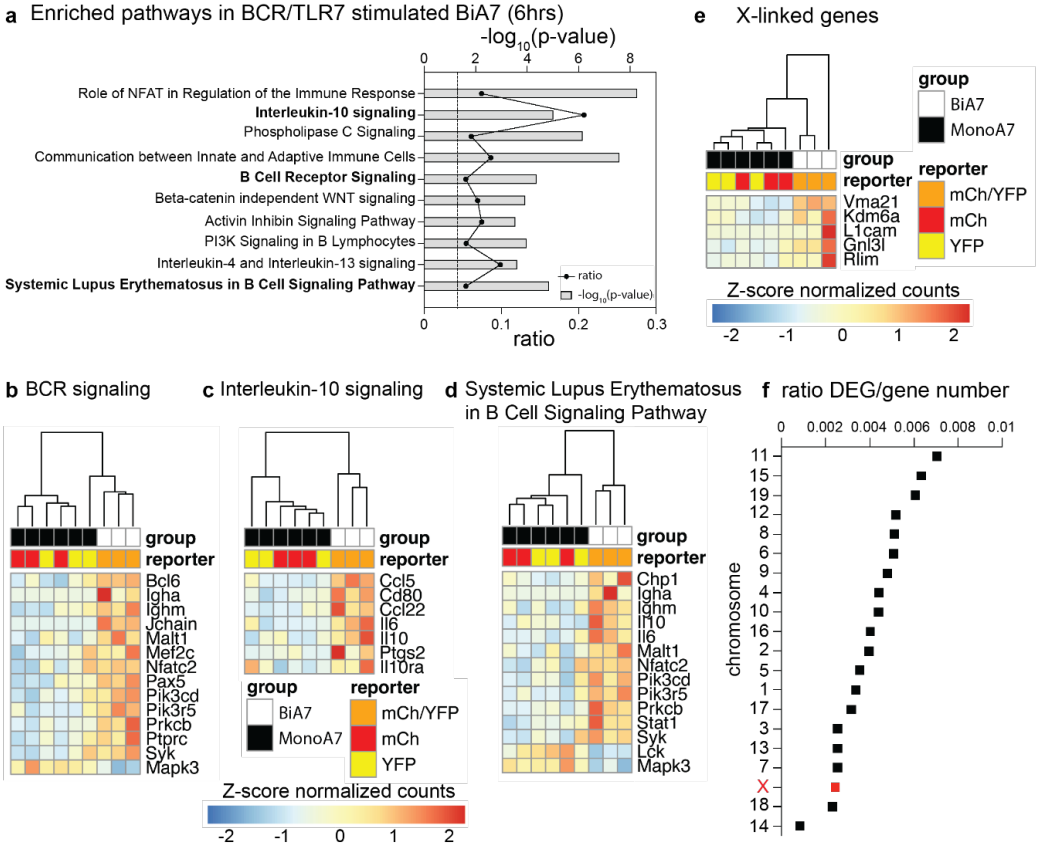

Extended data Figure 6. Early transcriptional changes upon activation of BiA7 B cells. CD19^{+}IgD^{+} sorted BiA7 and MonoA7 cells were stimulated with F(ab')$_2$ goat anti-mouse IgM, anti-CD40, CL097 for 6 hours and processed for RNA-seq analysis. (**a**) Up-regulated pathways in activated BiA7 B cells identified using ingenuity pathway analysis (IPA, QIAGEN). (**b - d**) Heatmap representing expression of DEGs from BCR signaling (**b**), IL10 signaling **(c)** and from Systemic Lupus Erythematosus in B cell IPA Signaling (**d**) Pathways in CD19^{+}IgD^{+} sorted BiA7 and mCh, YFP MonoA7 activated B cells. **(e)** expression of X-linked DEGs in BiA7 and MonoA7 activated B cells. **(f)** DEG/total gene number ratio for each chromosome.

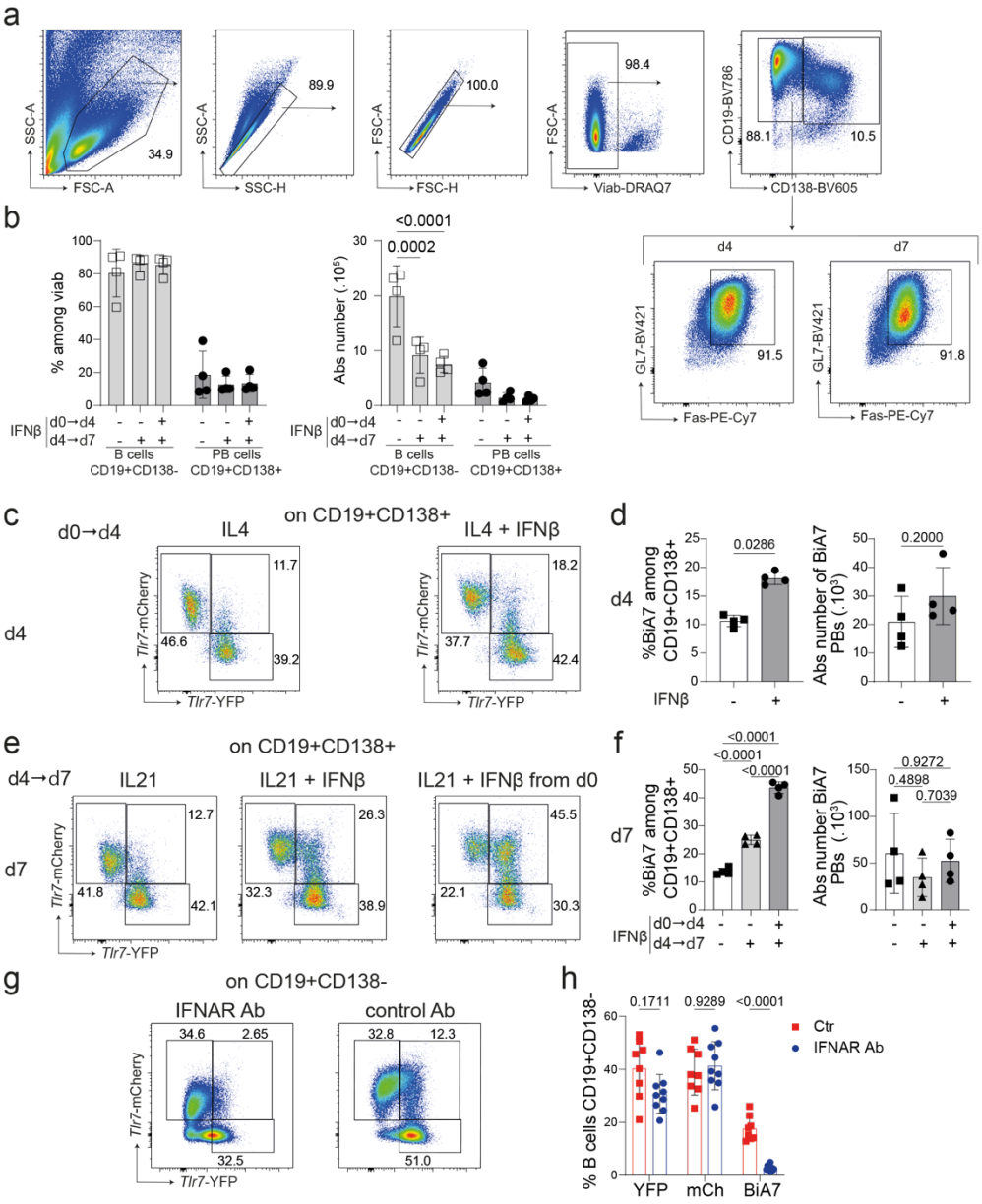

Extended data Figure 7: IFNAR1-signaling is required for the emergence of BiA7 B cells. (**a**) Gating strategy used for iGB cell analysis by flow cytometry. (**b**) Frequency and absolute number of $CD19^{+}CD138^{-}$ B cells and $CD19^{+}CD138^{+}$ PBs in iGB cell culture system with or without IFNβ. (**c-f**) Representative flow cytometry plots showing *Tlr7*-reporter expression in $CD19^{+}CD138^{+}$ PBs at d4 **(c)** and d7 **(e)** of iGB cell culture with or without IFNβ. Related histograms showing the frequency and the absolute number of BiA7 B cells among PBs at d4 (**d**) or d7 **(f)**. **(g, h)** Analysis of naive B cells from iGB culture with IL-4 alone for 4 days, then cultured with IL-21 and IFNβ in presence of IFNAR1 blocking or control antibody for 3 more days. Representative dot plot of *Tlr7*-reporter expression (**g**) and frequency of reporter expression (**h**) among $CD19^{+}CD138^{-}$ or $CD19^{+}CD138^{+}$ (PBs) cells. Data are representative of at least two independent experiments. Each dot represents an individual female mouse. Data are presented as mean ± SD. For (b**)**, Two-way ANOVA was performed followed by Tukey's multiple-comparisons test. For (d), Mann-Whitney test was used and for (f) One-way ANOVA was performed followed by Tukey's multiple-comparisons test. For (h), two independent experiments were pooled and a two-way ANOVA (Geisser–Greenhouse corrected) followed by Sidak's multiple comparisons test, was performed

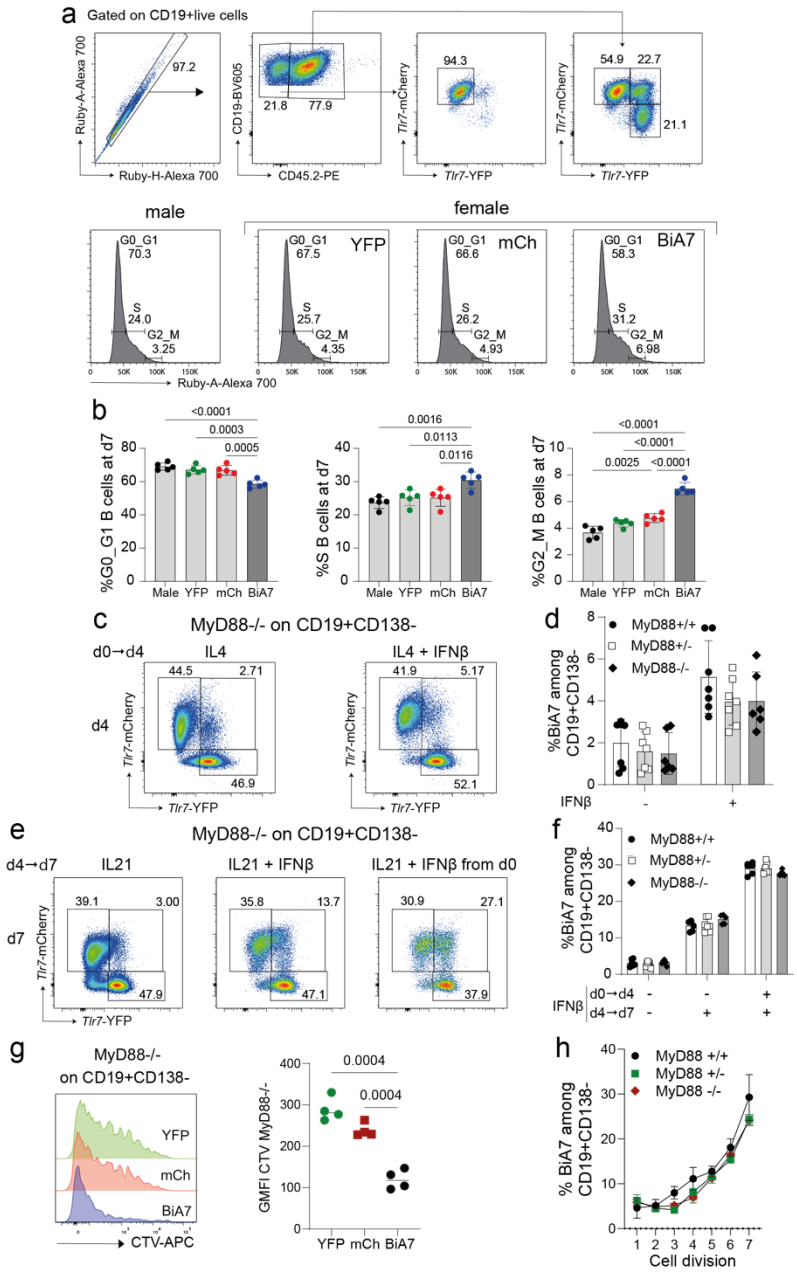

Extended data Figure 8: Myd88-signaling is dispensable for BiA7 B cell development *in vitro*. (**a,b**) Cell cycle analysis with Ruby staining of mix of ¼ male (CD45.1/CD45.1) and ¾ female (CD45.1/CD45.2) B cells in iGB cell cultures. Flow cytometry plot showing the gating strategy at d+7 (**a**). Analysis of DNA content in the indicated B cell using Ruby staining, and frequency of cells in each cell-cycle phases among male, MonoA7 and BiA7 female CD138- iGB cells at d+7 (**b**). (**c-f**) Analysis of MyD88$^{+/+}$, MyD88$^{+/-}$ or MyD88$^{-/-}$ purified B cells from dual reporter iGB cultures. Representative dot plots of *Tlr7*-reporter expression gated on CD19^{+}CD138^{-} B cells and frequency of BiA7 cells at d4 (**c,d**) or d+7 (**e,f**). (**g**) CTV dilution profile and CTV GMFI among CD19^{+}CD138^{-} B cells from dual reporter MyD88$^{-/-}$ mice. (**h**) Frequency of BiA7 B cells populations over cell division from MyD88$^{+/+}$, MyD88$^{+/-}$ and MyD88$^{-/-}$ dual reporter mice. Data are representative of at least two independent experiments. Each dot represents an individual mouse. Data are presented as mean ± SD. For (**b**) One-Way ANOVA was used with Tukey statistical hypothesis. For (**d,f**), two independent experiments were pooled and Two-way ANOVA was performed followed by Tukey's multiple comparisons test. For (g), paired RM one-way ANOVA (Geisser–Greenhouse corrected) was performed followed by Holm–Sidak multiple comparisons test.

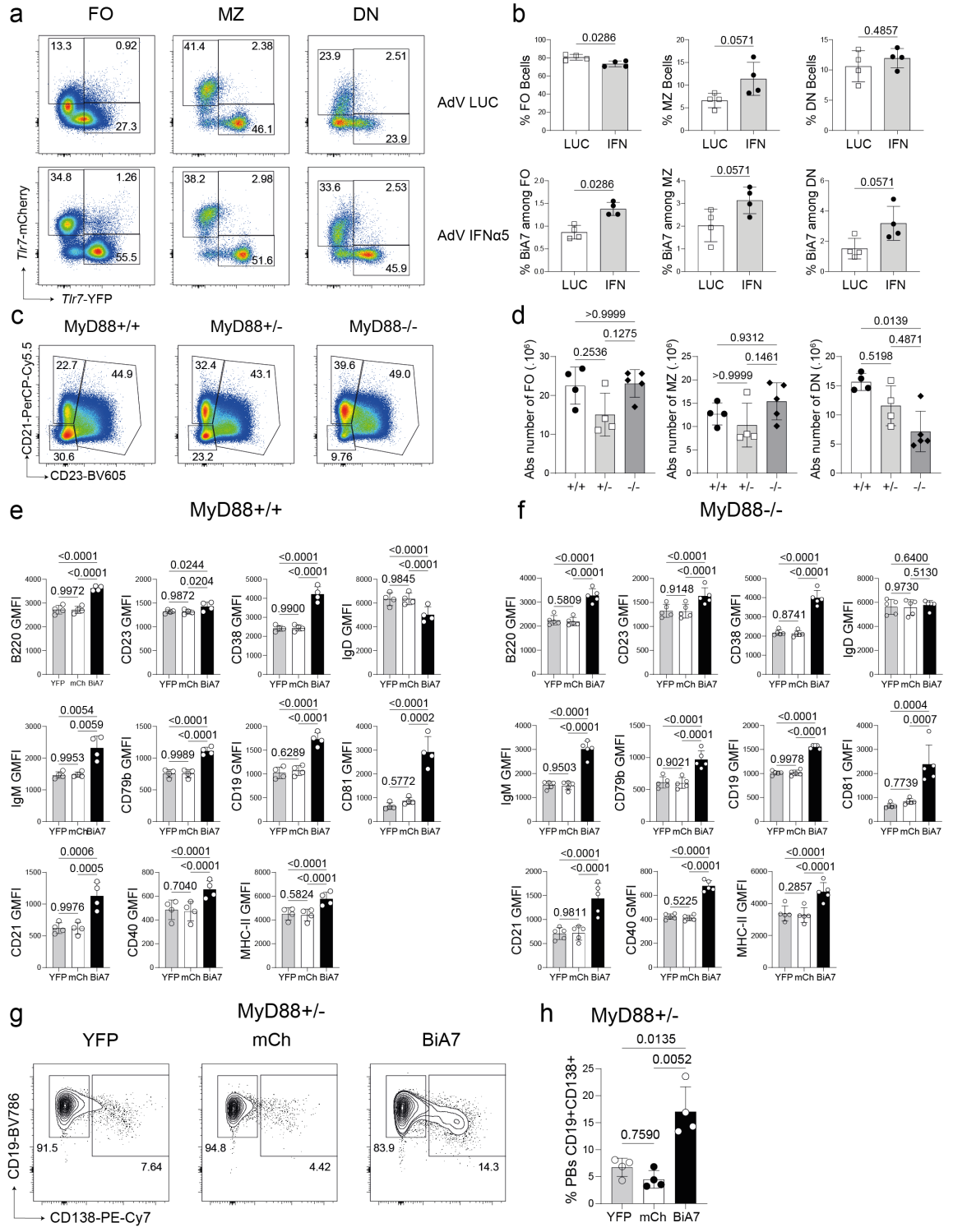

Extended data Figure 9: Impact of MyD88-deficiency on BiA7 B cell development among splenic B cell subsets. (**a-b**) Flow cytometry analysis of spleens from *Tlr7*-dual reporter mice harvested 2 weeks after i.v. injection of 10^7 ifu of AdV encoding either type I IFN (IFN-α) or Luciferase as control. Representative flow cytometry plots showing *Tlr7* reporter expression in FO, MZ and DN B cells subsets (**a**), frequency of each B cell subsets among $CD19^+$ cells and of BiA7 among each B cell subsets (**b**). (**c-h**) Flow cytometry analysis of splenic B cell subsets from *Rag2*-deficient mice sub-lethally irradiated and reconstituted with BM from either WT, $MyD88^{+/-}$ or $MyD88^{-/-}$ *Tlr7*-dual reporter mice, and i.v.

injected with AdV-IFN-α for 2 weeks. Representative flow cytometry plots (**c**) and absolute numbers (**d**) of FO, MZ and DN B cells subsets. (**e-f**) Histograms of individual GMFI of B cell markers gated on MonoA7 or BiA7 FO IgD^+ cells in reconstituted-$MyD88^{+/+}$ (**e**) or $MyD88^{-/-}$ (**f**) mice. (**g,h**) MonoA7 (either YFP or mCh) and BiA7 $CD19^+$ IgD^+ sorted B cells from $MyD88^{+/-}$ *Tlr7*-dual reporter chimeric mice were *in vitro* stimulated for 3 days with $F(ab')_2$ goat anti-mouse IgM, anti-CD40 and CL097. (**g**) Representative CD19 CD138 staining at day 3 and (**h**) frequency of *in vitro* differentiated $CD19^+CD138^+$ PBs. Data are representative of 2-5 independent experiments. Each dot represents an individual female mouse. Data are presented as mean ± SD. For (**b**), a Mann-Whitney test was used. For (**d**), a Kruskal-Wallis test followed by Dunn's multiple comparisons test was used. For (**e, f**), a paired one-way ANOVA followed by Tukey's multiple comparisons test and for(**h**), a paired one-way ANOVA followed by Sidak's with Sidak multiple comparisons test was used.

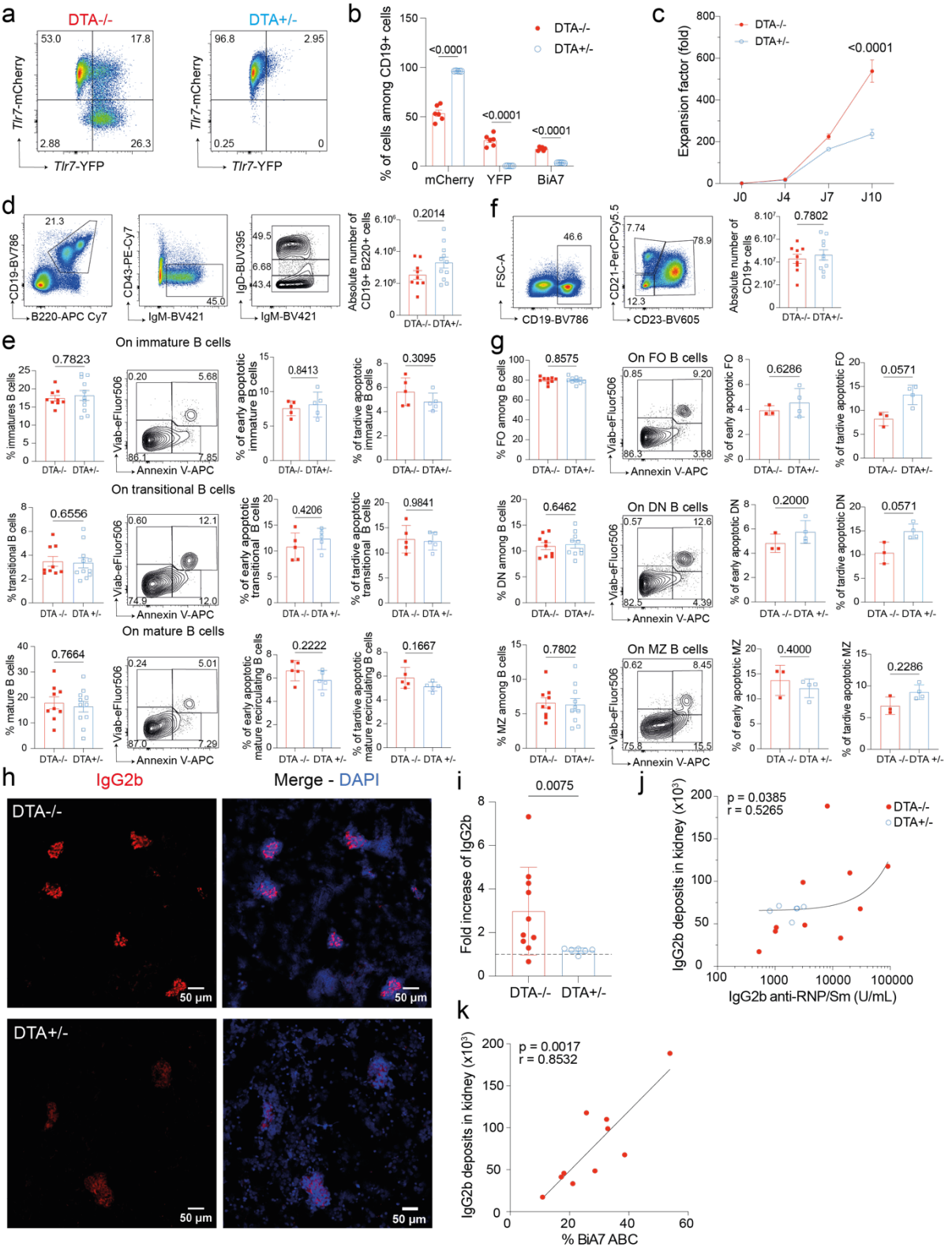

Extended data Figure 10: Enforced *Tlr7* mono-allelism has no significant impact on B cell development but protects from immunoglobulin deposits in the glomeruli in pristane-induced lupus-like disease. (**a-b**) Visualization of *Tlr7*-reporter activity in $CD19^+$ cells (**a**) and frequency of MonoA7 and BiA7 among $CD19^+$ cells (**b**) from $DTA^{-/-}$ and $DTA^{+/-}$ dual reporter mice cultured on 40LB stromal cells for 7 days (step1 no IFNβ; step 2 with IFNβ). (**c**) Cumulative fold increase in the number of $CD19^+$ iGB cells after step 1 & 2, and an additional culture with IL-21 and IFN-β from day 7 to 10. (**d-g**) Flow cytometry analysis of bone marrow (**d-e**) and splenic (**f-g**) B cell populations from $DTA^{-/-}$

and $DTA^{+/-}$ dual reporter mice. (**d**) Gating strategy for immature, transitional and mature B cells and absolute number of $CD19^{+}$ $B220^{+}$ cells in the bone marrow. (**e**) Frequency of immature, transitional and mature B cells among $CD19^{+}B220^{+}$B cells. Representative dot plot of annexin V/viab. dye staining profiles. Frequency of early and tardive apoptotic among immature, transitional and mature B cells. (**f**) Gating strategy of splenic FO, DN and MZ B cells and absolute number of $CD19^{+}$ cells. (**g**) Frequency of FO, DN and MZ B cells, representative dot plot of annexin V/viab. dye staining and frequency of early and tardive apoptotic among FO, DN and MZ $CD19^{+}$ B cells. (**h,i**) Kidney analysis 7 months post pristane injection of female $DTA^{-/-}$ and $DTA^{+/-}$ dual *Tlr7*-reporter mice. (**h)** Representative images of kidney sections stained for IgG2b (red). Nuclei counterstained with DAPI (blue). Scale bars, 50µm. (**i**) Fold increase of IgG2b deposits in pristane injected compare to not injected mice. Each symbol represents the mean of 20-160 glomeruli of individual mouse. (**j,k**) Correlation between the frequency of IgG2b deposits in kidney (**j**) and the titer of IgG2b anti-RNP/Sm in pristane-injected $DTA^{-/-}$ and $DTA^{+/-}$ mice (**j**) and the frequency of BiA7 IgD^{-} ABC cells in pristane-injected $DTA^{-/-}$ dual reporter mice (**k**). For (b-g, i), a Mann-Whitney tests were used. Spearman tests were used for correlations (j) and Pearson test for panel (k). The symbols represent individual mouse; bars represent the mean; the error bars represent the mean±SD. Data are representative of two independent experiments.